Holographic Back-Projection Method for Calibration of Fully Digital Polarimetric Phased Array Radar

David Schvartzman[iD], *Senior Member, IEEE*, José D. Díaz Díaz[iD],
Duŝan Zrnić[iD], *Life Fellow, IEEE*, Matthew Herndon[iD], *Member, IEEE*,
Mark B. Yeary[iD], *Fellow, IEEE*, and Robert D. Palmer[iD], *Fellow, IEEE*

Abstract—**Phased Array Radar (PAR) technology is rapidly rising as a candidate for future weather radars because it can provide focused, high-quality meteorological observations. Due to the need for precise measurements of polarimetric weather variables, it is desired that the radar simultaneously transmits and receives linearly polarized horizontal (H) and vertical (V) fields through beams that are well matched in gain and shape at every pointing direction. These scanning characteristics are difficult to achieve, especially with current methods such as the "park and probe" calibration, because the radiation patterns of PAR antennas are inherently dependent on their pointing direction. Thus, polarimetric array calibration is critical to produce matched H/V copolar antenna patterns. In this article, we present a polarimetric antenna calibration procedure for the fully-digital PARs based on the holographic back-projection of electric fields. The fully digital S-band Horus radar is used to implement and evaluate the proposed calibration method. First, near-field measurements of a fully active Horus antenna panel are back-projected onto the plane of the array to derive the copolar magnitude and phase of the H/V fields radiated by each antenna element. Then, digital calibration parameters are produced from back-projected fields to compensate for excitation differences and produce uniform radiation at the plane of the array. The performance of the back-projection calibration method is evaluated for broadside and for electronically scanned angles and compared to the more conventional park and probe calibration method. A robustness analysis is conducted using simulations to evaluate the impact of excitation amplitude and phase errors that could result from practical near-field environments and amplifier performance degradation. Preliminary results show that through precise digital calibration based on back-projected fields, beam matching can be significantly improved to achieve the desired polarimetric calibration levels. For electronically steered beams, back-projection calibration can reduce H/V beam mismatch biases by approximately 25%, from 0.34 dB to 0.08 dB. This improves measurement accuracy of fully digital PARs by mitigating antenna-induced biases in meteorological estimates.**

Index Terms—**Phased array radar, radar calibration, polarimetric radar, digital radar, weather radar.**

I. INTRODUCTION

PHASED Array Radar (PAR) technology offers advanced capabilities that can support enhanced weather surveillance strategies to improve the volume update time and quality of observations. Hence this technology is an attractive candidate for the future generation of weather radars. However, there are challenges to precise measurements of polarimetric variables. For example, it is crucial that the beams for transmitting the Horizontally (H) and Vertically (V) polarized waves are well matched in shape and gain at every pointing direction. Similarly on reception, the shapes, as well as gains of H and V beams, must be matched, ideally without cross-coupling between the two orthogonal polarization channels. These demands are hard to achieve because radiation patterns of phased array antennas are inherently dependent on the element level polarization. Therefore, shape and gain are functions of the pointing direction and so is the polarization at the location of weather observations. As an example, arrays of patch antenna elements (common because of their low cost and relatively easy design) produce orthogonal H and V fields only in the principal planes of the array, whereas the radiated fields increasingly depart from their intended polarization in other directions. This causes rising levels of cross-polar patterns on transmit and receive as beams are steered away from the principal planes. The presence of these and other related practical effects can distort the H and V beams, introducing significant biases in the estimates of polarimetric variables.

The variables driving the requirements for the accuracy of polarimetric measurements are differential reflectivity (Z_{DR}), specific differential phase (K_{DP}), and copolar correlation coefficient (ρ_{hv}). By definition Z_{DR} is the logarithm of the horizontal (H) to vertical (V) returned powers ratio, K_{DP} is the derivative of the differential phase (Φ_{DP}) with respect to range, Φ_{DP} is the phase difference between the signals of H and V polarized waves along a radial up to a specified range, and ρ_{hv} is the normalized correlation coefficient between the

received H and V signals. To accurately estimate rainfall rates, it is recommended that the bias of Z_{DR} is kept within ± 0.1 dB for intrinsic Z_{DR} between 0 and 1 dB and less than $0.1 \times Z_{DR}$ for larger Z_{DR} values [1], [2]. This imposes strict polarimetric calibration requirements to closely match the far-field copolar H and V beams [3]. It is noted that keeping the bias of Z_{DR} estimates within ± 0.1 dB is difficult even on radars with parabolic antennas, and for this reason, the bias accuracy to within ± 0.2 dB for Z_{DR} less than 1 dB (and up to $0.2 \times Z_{DR}$ for larger Z_{DR}) is accepted as a more realistic goal at this time [1]. Concerning ρ_{hv} estimates, a bias within ± 0.01 is deemed sufficient for "sensing the mixed-phase precipitation and gauging the hail size quantitatively" [4], however, the latest requirements specify a desired bias within ± 0.006 [2]. For these reasons, polarimetric calibration of phased array radars is of critical importance to the success of this technology in weather observations [5].

Ongoing efforts are focused on investigating polarimetric PAR calibration methods to produce accurate weather observations. The calibration of phased array antennas requires the determination of the aperture distribution of the antenna for a given set of excitation coefficients. Calibration methods used can be classified in three categories: 1) based on near-field pattern measurements, 2) based on far-field pattern measurements, and 3) based on in-situ measurements. Near-field measurements taken in anechoic chambers can align the array via a conventional park-and-probe method [6]. Thereby, magnitudes and phases of copolar pattern peaks of each element are measured to derive beamforming coefficients that equalize the array (i.e., uniform magnitudes and phases). Although this can provide coefficients for "initial calibration", it is not accurate enough for polarimetric weather measurements as it fails to capture the total radiated energy, especially outside the array plane. Far-field measurements can be used to map full array patterns and derive coefficients to equalize magnitudes and phases at the copolar peaks [7], [8]. However, obtaining far-field range measurements requires a fully articulated antenna pedestal to enable the array to rotate and allow calibration of every beamsteering position. Furthermore, far-field measurements are sensitive to external contamination like multi-path reflections and interfering signals [9], [10]. A new promising method that could mitigate these problems is measurement with an unmanned aerial system (UAS) capable of transmitting/receiving radar signals while flying in the far-field [11], [12]. Possible issues are restrictions imposed by federal agencies that may limit the aperture size that can be measured. Lastly, in-situ calibrations independent of external infrastructure, like the mutual-coupling [13], and the weather-based method [14], are promising. Nevertheless, mutual-coupling provides relative calibration coefficients that can bring the array to an absolute calibration state. Therefore, its accuracy depends on that from the absolute calibration. At some pointing directions, some variables can be calibrated using weather returns; for example Z_{DR} can be calibrated in the principal planes using returns from Bragg stutterers or drizzle [15], [16]. But for radar reflectivity (Z_h), absolute calibration is needed. None of the described methods has been shown to achieve polarimetric

PAR calibration that meet requirements for accurate weather measurements [2].

Herein, we present a new polarimetric PAR calibration method that relies on holographic back-projection to derive electric-field magnitudes and phases radiated by each antenna element [17], [18]. Although this method has been previously considered for PAR calibration [19], it has not been evaluated for fully-digital polarimetric PAR with the goal of achieving accurate beam matching for meteorological observations. This is critical for recommending the adoption of polarimetric PAR technology for the future nationwide network of polarimetric radars in the U.S. Further, back-projection has not been used to calibrate accurately and simultaneously both, amplitudes and phases of each individual antenna element in a polarimetric array. This is mainly due to the difficulty in applying high precision coefficients using (analog) phase shifters and attenuators on non-fully digital arrays, and that fully digital PAR technology is only starting to become available. Lastly, we conduct an evaluation of the robustness of polarimetric back-projection calibration to excitation errors (amplitude and phase), and derive a new metric, the "Beam Mismatch Contamination" to quantify its effectiveness.

The analysis presented in this article uses holographic E-field back-projections to compensate excitations and produce symmetric, well-matched H/V far-field patterns that mitigate copolar beamsteering biases. One antenna panel of the S-band mobile polarimetric fully digital Horus radar system is used to evaluate the performance of the proposed calibration method in a near-field anechoic chamber [20]. Nevertheless, this method is not specific to the Horus radar and could be applied to other PARs, although we expect the performance to improve as the total number of digital channels increases. A companion article providing an in-depth technical description of the Horus system can be found in this journal [21]. Furthermore, an article evaluating the performance of the Horus antenna patterns on the copolar correlation coefficient (ρ_{hv}) is also in this special issue [22].

This article is organized as follows. Section II, introduces the fully digital Horus system for which the calibration method was developed. Section III, describes the near-field planar scanner that measures the Horus antenna, and the near-field to far-field transformation procedure. Section IV, introduces the back-projection method and provides results from actual Horus near-field measurements. Section V discusses the application of this method to improve PAR polarimetric calibration. A robustness evaluation using actual measurements with systematically simulated amplitude and phase excitation errors is conducted in Section VI. The conclusion of this work is provided in Section VII.

II. THE FULLY DIGITAL HORUS RADAR

The U.S. is safeguarded by a network of approximately 160 S-band, polarimetric weather radars, which are maintained and operated by the National Oceanic and Atmospheric Administration (NOAA). The WSR-88D stands for "Weather Surveillance Radar - 1988 Doppler" and will be reaching end of life by 2040. The WSR-88D is considered the "golden standard" in the meteorological community. Phased

Fig. 1. Photograph of the mobile, fully digital, S-band polarimetric phased array radar called "Horus." The system consists of 25 panels each with 8 × 8 dual-polarization elements (1,600 polarimetric elements in total).

TABLE I
SPECIFICATIONS OF THE HORUS RADAR

Frequency	2.7–3.1 GHz
Polarization	ATSR/STSR/RHCP/LHCP
Tx Waveform	Arbitrary Waveform Generator
Tx Peak Power (single element)	10 W/polarization
Max Tx Pulse Width	100 μs @ 10% duty cycle
Max Tx Bandwidth	100 MHz
Element Spacing	0.5 λ @ 2.951 GHz
Number of Panels	25 (1600 elements)
Max Electronic Scan Angle	$\pm45°$ az, $\pm45°$ el
Aperture Size	2.03×2.03 m^2
Tx/Rx Beamwidth Broadside	2.58° (no taper, one way)
Detectability (1 pulse)	4.3 dBZ @ 50 km

Fig. 2. Near-field scanner setup to fully characterize the H and V antenna patterns of the Horus system with (a) front (b) back view.

array radars are being considered as a potential replacement technology for the WSR-88Ds, but the data quality and overall performance must meet or exceed that of the WSR-88D radars.

The most advanced architecture for a phased array radar is a fully digital design [23]. In such architectures, every element and polarization has its own transmitter and receiver and is usually quite flexible in terms of software reconfigurability. In collaboration with NOAA's National Severe Storms Laboratory (NSSL), the Advanced Radar Research Center (ARRC) at the University of Oklahoma (OU) has recently completed the S-band mobile polarimetric fully digital "Horus" radar system shown in Fig. 1 [21], [24]. This radar is considered an *engineering* demonstrator with the goal of mitigating risks associated with fully digital phased array architectures and demonstrating advanced capabilities. Its size and operating frequency (see Table I) limit the beamwidth to ∼4° (i.e., with taper), which is not adequate to resolve for most weather applications. However, its inherent scalable design allows the demonstration of overall functionality while considering plans for future full-scale systems.

The fundamental building block of Horus is a fully digital, dual-polarization array panel made up of an 8 × 8 mechanical and electrical subarray (see Fig. 2). The array frame for the panel provides mechanical support as well as a conduit for liquid cooling. The "OctoBlades," eight used per panel, house all the electronics. An OctoBlade can be hot-swapped into a panel to provide all electrical connections, liquid cooling, and connection to the radiating elements via blind-mate conn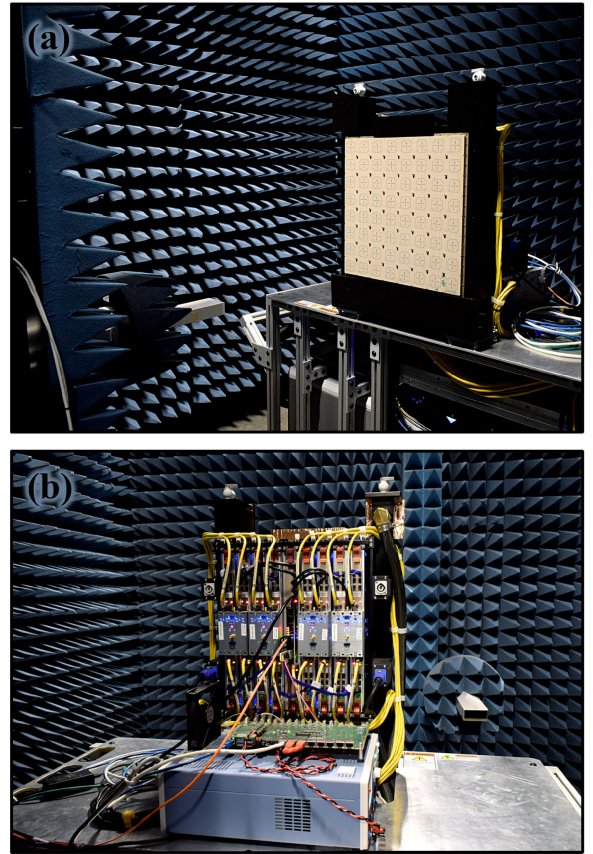ectors. The OctoBlades can easily be moved (e.g., Line Replaceable Unit (LRU)) to different positions in the array and are designed to automatically recognize their position, orientation, calibration weights, etc.

Each panel also contains a so-called "SuperBlade," that supports the OctoBlades with DC power, local oscillator signal, and reference clock. Operating with waveforms in the 2.7–3.1 GHz band (switchable from dwell-to-dwell), the aperture-coupled, stacked-patch radiating elements provide high polarimetric isolation (greater than -45 dB cross-polarization suppression after calibration) [25]. Another important feature of fully digital arrays is the potential for mutual-coupling-based array calibration, which has been demonstrated by the ARRC team [26].

This paper focuses on the precise near-field calibration of the fully digital Horus panel. The calibration results shown next are from the single panel with fully populated electronics with 8 OctoBlades and a SuperBlade. Given the scalable design of Horus, these results represent the performance level expected with any larger-size Horus radar.

III. NEAR-FIELD MEASUREMENTS

To enable testing of Horus system electronics, one panel of OctoBlades (128 total digital channels, 64 per-polarization) was connected to an 8 × 8 dual-polarization antenna panel. This panel was placed into a custom-built near-field chamber (Fig. 2) lined with RF absorber. Then, it was integrated with a coherent digital channel separate from the panel electronics. Transmit and receive mode near-field measurements are made

using the off-panel channel, which is connected to a standard gain S-band open-ended rectangular waveguide probe (OEWP) covered with a collar of RF absorber and attached to a two-axis positioner. The scanner assembly is comprised of two Velmex BiSlide assemblies driven by stepper motors and one Velmex VXM stepping motor controller for coordinating their movements, all mounted on a Newport "optical breadboard" base to achieve precise leveling. Although the OEWP is a single-polarization antenna, its polarization axis is precisely controlled, allowing repositioning to measure copolar patterns of either polarization, or both simultaneously (0°, 90°, and 45°). This near-field setup gives space for the panel to operate as a radar (albeit with a small aperture) within a pristine environment for both calibration and performance testing in either receive or transmit mode, and enables accurate antenna radiation pattern characterization for the H and V polarizations.

In this near-field setup, precise 3D alignment between the antenna aperture and the 2D scanning plane is achieved using laser alignment. A laser fastened to the OEWP matches the normal of the scanner plane and provides an alignment reference for the panel used both when centering the scanner on the antenna under test (AUT) and when correcting for any residual angle between the scanner plane and array face. To align the array face and the scanner plane, the array is first positioned at a fixed distance from the face of the OEWP and aligned with the scanner using the laser. Next, any residual angle between the scanner and array planes is corrected by adjusting four risers on the antenna platform until the surfaces are parallel to within a tolerance of ±0.1° (measured using a digital level sensor).

Finally, the precise distance from the face of the OEWP is measured using a Leica Distro X3 laser rangefinder (accurate to within ±1mm) for later use during back-projection.

Our near-field calibration uses a park-and-probe technique to measure amplitudes and phases at each digital channel (128 in total). Then, it generates and applies alignment weights. Lastly, it verifies the resulting alignment. A full set of transmit patterns (co- and cross-polar H and V patterns) requires four separate data collections, one for each combination of array polarization and OEWP orientation (0° or 90°). Because the OEWP is linearly polarized, it is impossible to separate the H- from the V transmit response if the Horus antenna transmits both polarizations simultaneously. Receive patterns can be obtained with only two sets of scanner measurements. The panel hardware can receive both polarizations simultaneously and independently process the data. Multiple beam angles can be collected simultaneously on receive.

A. Near-Field Samples and Far-Field Transformation

Near-field data was acquired for all 128 channels (i.e., 64 H- and 64 V-pol) setting the OEWP in transmit and the Horus 8 × 8 in receive mode. Figs. 3 and 4 show the measured co- and cross-polar near-field patterns for the H-polarization in the array; white squares indicate the antenna element positions.

A mathematical transformation and a correction for the effects of the measuring probe is used to determine the far-field radiation patterns of the antenna from the near-field measurements. Next we summarize the mathematical expressions
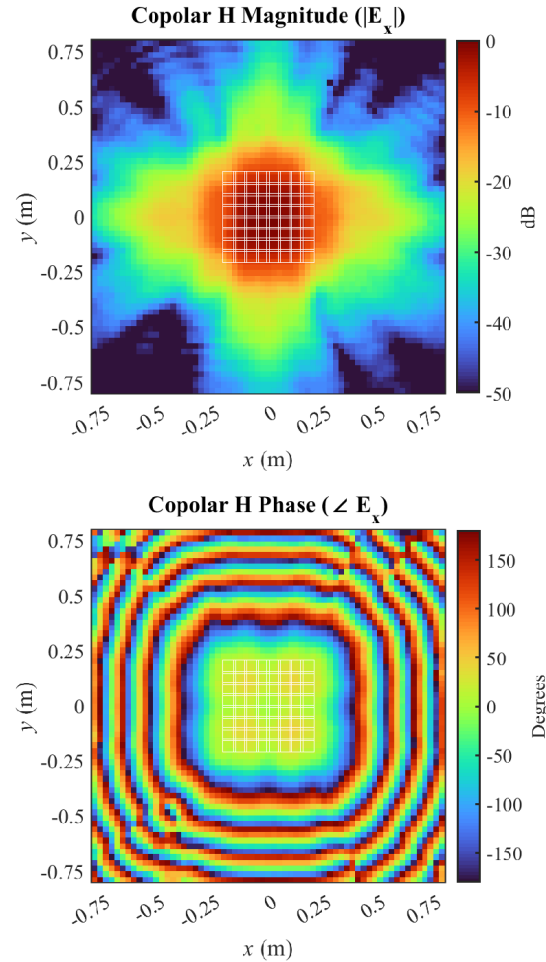

Fig. 3. Copolar planar near-field measurements of the H polarization sampled at 3λ from the Horus antenna panel (top) E-field intensity, and (bottom) phase.

from [27], needed to transform the near-field measurements into far-field patterns.

Near-field and far-field patterns are Fourier transform pairs [27]. First, assume the measured near-field samples are represented by,

$$E_{xa}(x, y, z = 0) = \frac{1}{4\pi^2} \int_{-\infty}^{+\infty} \int_{-\infty}^{+\infty} f_x(k_x, k_y) \, e^{-j(k_x x + k_y y)} \, dk_x dk_y,$$

(1)

where $E_{xa}(x, y, z = 0)$ is the measured electric near-field in the x direction (parallel to the ground) sampled in the xy plane parallel to the AUT at the location of the probe ($z = 0$), $f_x(k_x, k_y)$ represents the plane wave spectrum of the field, and k_x and k_y are the spatial wavenumbers (see eqs. 17-13 a and b in [27]). Similarly, the y component of the near E-field is,

$$E_{ya}(x, y, z = 0) = \frac{1}{4\pi^2} \int_{-\infty}^{+\infty} \int_{-\infty}^{+\infty} f_y(k_x, k_y) \, e^{-j(k_x x + k_y y)} \, dk_x dk_y.$$

(2)

The x and y components of the plane wave spectrum, $f_x(k_x, k_y)$ and $f_y(k_x, k_y)$, are determined by Fourier

Cross-Polar H Magnitude ($|E_y|$)

Cross-Polar H Phase ($\angle\,E_y$)

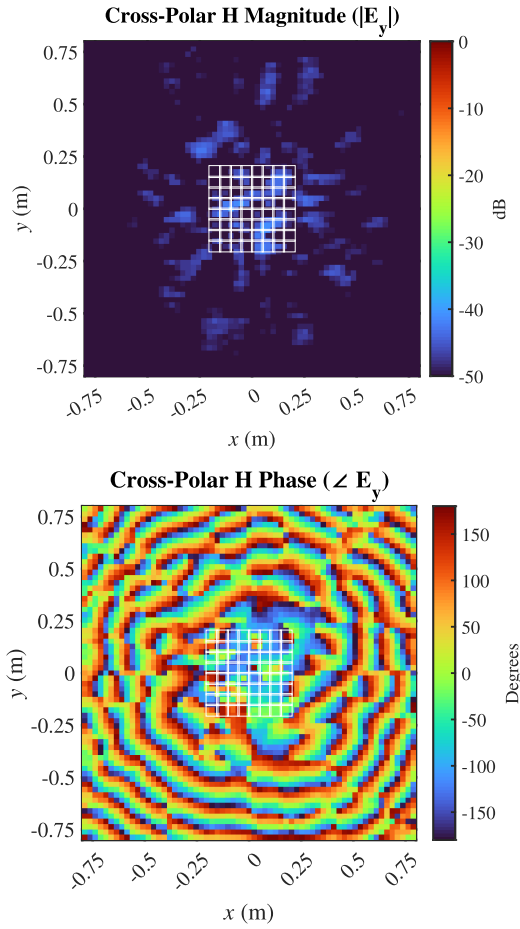Fig. 4. Same as Fig. 3, but for the cross polarization field.

transforming the measured near-zone E-fields (1) and (2), [27]

$$f_x(k_x, k_y) = \int\limits_{-b/2}^{+b/2}\int\limits_{-a/2}^{+a/2} E_{xa}(x', y', z' = 0)\ e^{j(k_x x' + k_y y')}dx'dy', \tag{3a}$$

$$f_y(k_x, k_y) = \int\limits_{-b/2}^{+b/2}\int\limits_{-a/2}^{+a/2} E_{ya}(x', y', z' = 0)\ e^{j(k_x x' + k_y y')}dx'dy', \tag{3b}$$

where a and b are the width and height of the measurement plane.

The far-field patterns in the antenna-relative spherical coordinate system θ, ϕ, can be expressed in terms of the plane wave spectrum of equation (3a) and (3b) as

$$E_\theta(R, \theta, \phi) \simeq j\frac{ke^{-jkR}}{2\pi R}(f_x \cos\phi + f_y \sin\phi), \tag{4}$$

$$E_\phi(R, \theta, \phi) \simeq j\frac{ke^{-jkR}}{2\pi R}\cos\theta(-f_x \sin\phi + f_y \cos\phi), \tag{5}$$

where R is the range where the far-field radiation pattern is estimated (i.e., $R \gg 2D^2/\lambda$) and k is the wave number $2\pi/\lambda$. After discretizing the spatial dimensions, a finite-sampling version of this transformation can be applied directly to the near-field samples measured over a finite sampling grid (see [27]). It results in antenna far-field patterns that include

effects of the measurement probe, which must be removed prior to calibration processing.

B. Probe Correction

The far-field patterns acquired through a near-field measurement must be corrected to account for the interaction between the AUT and the measuring probe. This interaction especially affects the measurement of the cross-polarized radiation outside of the principal planes. Herein the compensated far-field patterns E_p and E_c are given by [28],

$$E_p = \frac{E_{pp,2}E_{pu} - E_{cp,1}E_{cu}}{E_{pp,1}E_{pp,2} - E_{cp,1}E_{cp,2}} \tag{6}$$

$$E_c = \frac{-E_{cp,2}E_{pu} + E_{pp,1}E_{cu}}{E_{pp,1}E_{pp,2} - E_{cp,1}E_{cp,2}}, \tag{7}$$

where the subscripts "pp" and "cp" refer to the copolarized and cross-polarized responses of the probe, "pu" and "cu" to the uncompensated far-field radiation patterns of the AUT, and "1" and "2" to the alignment of the probe with respect to the measured fields. Notice that only one set of co- and cross-polarization patterns are required for the probes. This is because the 90° rotation between probe 1 and probe 2 imposes $E_{pp,2} = E_{pp,1}(\phi + 90°)$. The probe electric fields were generated using the dimensions of the OEWP employed in the measurements. The electric fields come from the closed-form solutions (through spectral techniques) for a slot in an infinite ground [28], [29]. Considering that these are standard probes delivered with professional near-field scanning systems, which also use these ideal patterns for probe correction on conventional near-field measurements, we consider the ideal probe-correction methods assumption to be sufficient. Furthermore, these probes have a very wide beam compared to the array panel, therefore, corrections based on probe-pattern measurements would not have significant effects in the measured array patterns. Once these fields are acquired, the corresponding co- and cross-polarization components are estimated and introduced as corrections in (6) and (7).

Equations (1) through (5) are applied to the Horus vertical and horizontal near-field measurements, then (6) and (7) compensate for the measuring probe using the fields of the OEWP. That way the far-field radiation patterns of this 8×8 array are obtained (i.e., one Horus panel). Cross-normalized far-field patterns of the H and V polarizations are presented in Fig. 5. In this case, the absolute gain of the copolar V pattern is 0.069 dB higher than the gain of the copolar H pattern.

A qualitative comparison of these patterns indicates excellent mainlobe alignment of the H and V patterns up to about -20 dB (i.e., $-12.5° \leq \theta \leq 12.5°$). The sidelobe structure for each polarization appears to be symmetric around the mainlobe for the horizontal and vertical cuts. A small difference (≤ 0.7 dB) is between peak sidelobe levels in the H and V patterns. This may be caused by truncation effects or mutual coupling [30]. Similarly, in the diagonal plane cuts the H and V mainlobes are well matched (down to about -20 dB), but sidelobes are lower than those in the principal planes (as expected) due to the rectangular antenna geometry.
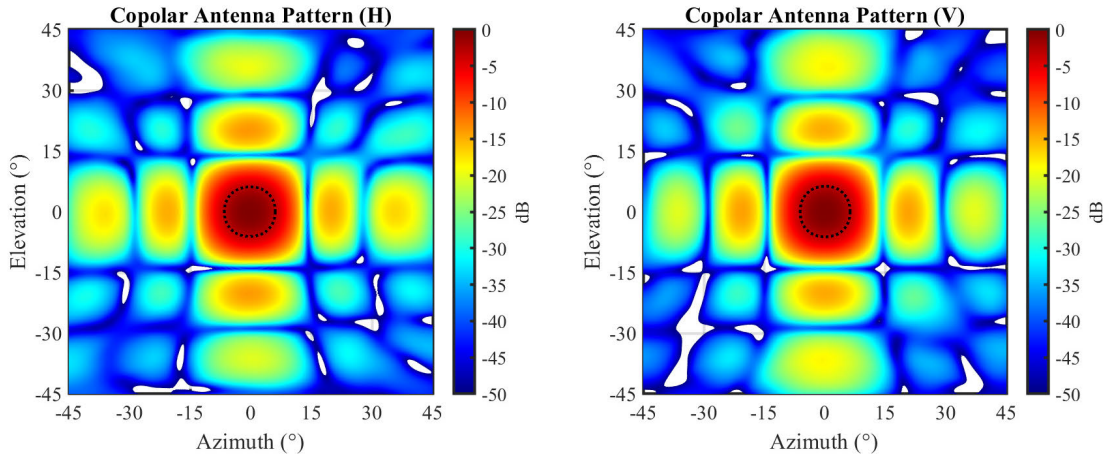
Fig. 5. Cross-normalized far-field probe-corrected antenna patterns derived using the near-field to far-field transformation. In this case, the absolute gain of the copolar V pattern is 0.069 dB higher than the gain of the copolar H pattern. Note that only park and probe alignment was used to produce these patterns. Dotted black contours represents the -3 dB widths of the copolar H and V patterns.

IV. BACK-PROJECTION METHOD

The holographic back-projection allows the evaluation of electric radiated near-fields to determine their characteristics (i.e., magnitude and phase) as they propagate in space. This, however, approximately holds in the reactive near-field where evanescent modes cannot be reproduced due to their complete attenuation at the probe's measuring distance. The method back projects the measured near-field patterns to the aperture surface of the array and then forms an estimate of the aperture excitation (magnitude and phase) distribution on the array plane [31]. The accuracy of the method is naturally limited by array performance, excitation stability, and the quality of the near-field environment. Furthermore, due to finite resolution and truncation effects, the traditional implementation of this method has been applied to high directivity phased array antennas to investigate feeding network anomalies, sources of cross-polarization radiation, or detection of faulty elements. Nevertheless, [32] found that the error contributions from field truncation in the holographic back-projection method are minor compared to other listed sources of error. These encouraging results motivate investigating the effectiveness of this method for calibrating upcoming fully digital polarimetric arrays.

For the Horus radar, 16-bit precision digital-to-analog converters (DACs) are used before the antenna front-end in the fully digital implementation [21]. This enables precise control of element-level beamforming coefficients for calibrating the transmit/receive excitations. We use the expressions (1) through (5) to take the Horus near-field measurements back to the array plane which is at a negative range r from the measurement plane (i.e., the distance from the measuring probe to the antenna). Note that the probe position has to be estimated accurately in 3D space for the holographic back-projection method to work. Further, near-field sampling should be aligned with the center of each element in a uniform grid.

Back-projected E-field magnitudes and phases for the co- and cross-polar H patterns are shown in Figs. 6 and 7. As in Figs. 3 and 4, element locations are delineated with white contour lines. A qualitative analysis of the top panel in Fig. 6 indicates that most of the energy from the measured fields is back-projected on top of the element locations in the array, with well defined power-level transitions (i.e., $\sim$0 dB to ~-20 dB) right along the edges of the panel. Apparent diffraction fields can be observed propagating outwards around the panel. These seem to be particularly stronger in the x direction, aligned with the wave polarization being measured (H). Similarly, back-projected phases shown in the bottom panel of Fig. 6 appear to be close to 0° on the elements. Note that these are raw phase estimates, wrapping in the $\pm180°$ interval. Cross-polar field back-projections in Fig. 7 show higher intensity values around the edges of the panel (especially in the corners), and a non-smooth phase field across the panel.

There are several advantages of this method compared to other approaches. First, near-field measurement systems can be used to collect multiple beams at different frequencies over the course of a single data scan. This significantly reduces measurement time when using continuous probe motion scans. Further, this calibration method uses the entire active aperture and captures mutual coupling, scattering and reflections from the array structure, and temperature effects that may go undetected using the previously discussed park & probe method. However, some limitations that must be deliberated fare as follows.

For the method to be effective, a) the antenna must be properly aligned so that the array aperture is parallel to the measurement scan plane prior to the calibration process and b) the measurement scan deviations from the plane should be lower than $(1/100)\lambda$ [18]. An adequate size scan plane is required to capture significant E-field energy ($>$90% [33]) and thus minimize truncation errors. This requires a scan plane larger than that used to measure initial alignment coefficients (i.e., obtained via park & probe). Errors induced in E-field holograms due to truncation were quantified by [34] to facilitate scanner design considerations for accurate measurements. For this method to be effective, it is critical that the reference excitations remain stable while measuring all elements for a particular array operating mode and environment. This can be challenging for large arrays, or arrays without precise control of temperature gradients across the aperture. Lastly, due to
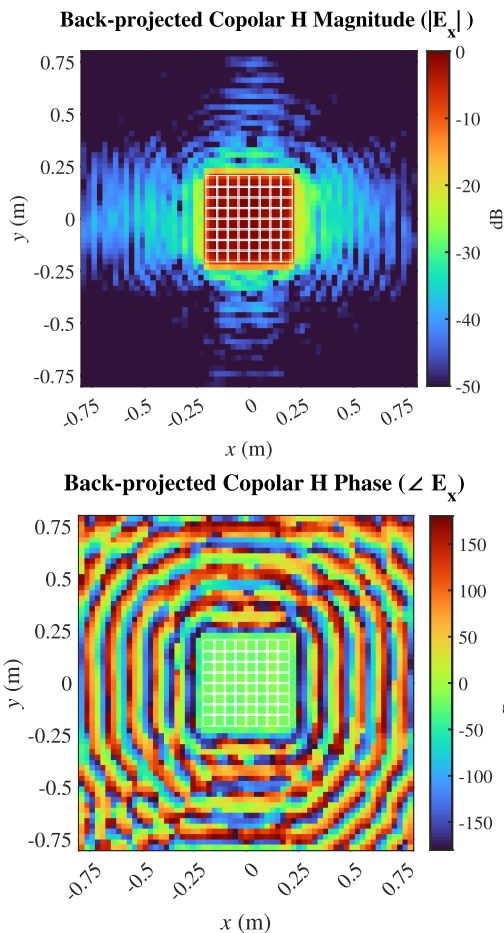
Fig. 6. Back-projected copolar H fields on the antenna plane (top) intensity, (bottom) phase.

Fig. 7. Back-projected cross-polar H fields on the antenna plane (top) intensity, (bottom) phase.

the non-linear nature of PAR amplifiers, deriving excitations corrections using back-projection may require an iterative process. Although feasible, this may be more time consuming. The number of iterations needed would depend on amplifier linearity and its operating point (i.e., near saturation).

We propose using back-projected fields (H and V) to perform polarimetric array calibration in an iterative excitation adjustment approach. That is, since the sampled near-fields capture most of the radiated energy, we argue that calibration based on back-projected fields can accurately compensate for element-level excitation differences in magnitude and phase. Initial results are presented next, along with a simulation-based robustness evaluation of the back-projection polarimetric calibration method.

V. POLARIMETRIC CALIBRATION

The holographic back-projections of near-field measurements at the H and V polarizations are used here to perform polarimetric calibration with the goal of improving beam matching. To this end, the x and y components of back-projected fields estimated from the physical center of the antenna elements are extracted.

A. Broadside Beams

Copolar back-projected excitations for broadside beams are shown in Fig. 8. In the copolar H magnitude and phase
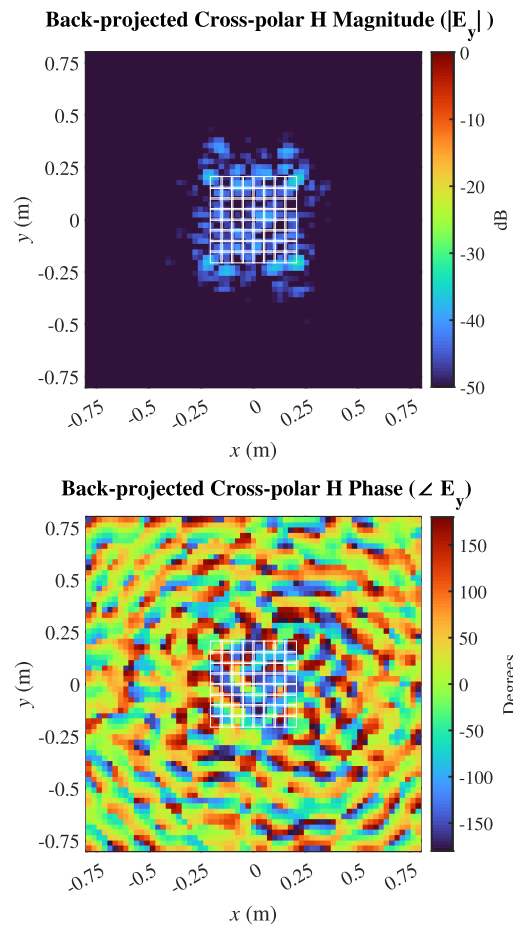
fields, the standard deviations are 0.47 dB and 2.15° across all 64 elements. Similarly for the copolar V fields, the standard deviations are 0.53 dB and 2.33°. These variations are due to several practical effects, mainly controlled by amplifier stability in saturation, truncation, and field diffraction around the array.

Ideally, the magnitude and phase of fields radiated by each element should be 0 dB (normalized) and 0° for accurate broadside beam forming. To achieve this we use the back-projection excitation estimates. Thus we derive a set of magnitude and phase weights so that radiated electric fields are uniform, i.e., 0 dB magnitudes and 0° phases across the array. We apply these small calibration corrections to the fields on the antenna elements and project the corrected fields (including radiation outside of the panel) forward via the traditional near-field to far-field transformation (see Section III).

We use the difference in copolar H and V beam patterns as a quality metric to evaluate beam matching. Pattern differences measured after park & probe alignment only (from Fig. 5) are presented in the left panel of Fig. 9 where the dotted black line represents the −3 dB beamwidth of the H pattern. Because the design of the microstrip patch antennas is symmetric, one would expect the far-field beams at the H and V polarizations to be relatively well matched. However, due to the calibration and finite array effects, coupled with practical fabrication imperfections, there are differences in the copolar patterns.
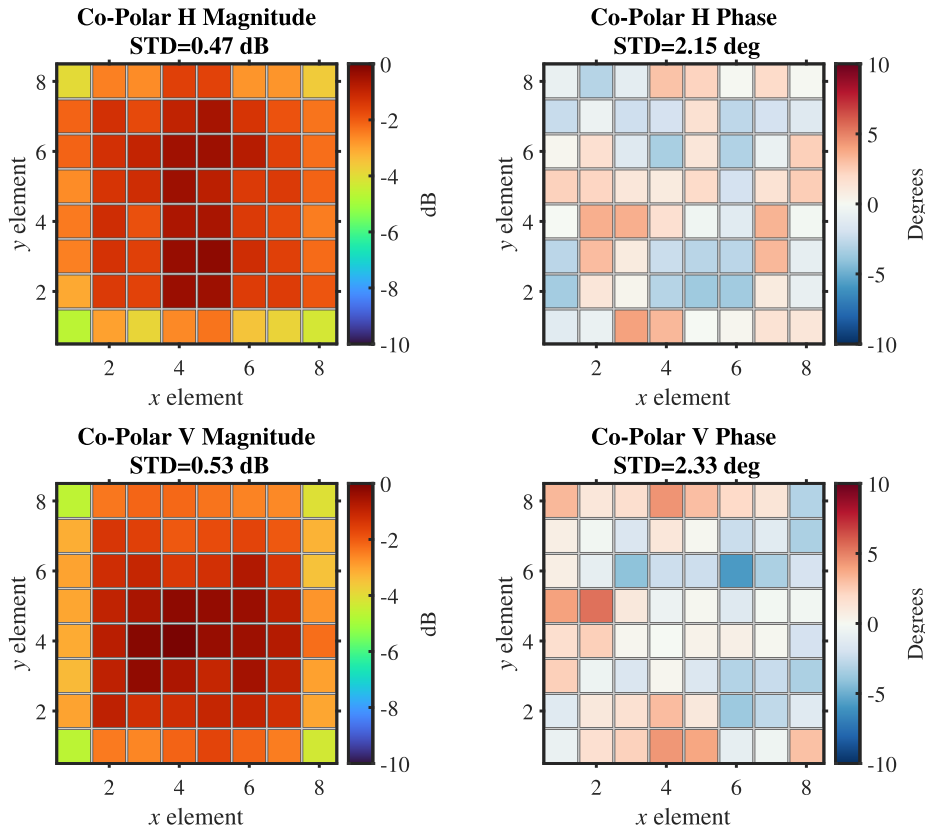
Fig. 8. Magnitude and phase of copolar fields back-projected on the array plane (top row) H (bottom row) V.

These can introduce significant biases in the polarimetric variables, especially as the beam is steered off broadside. Application of the back-projection-based correction mitigates these issues. The resulting copolar H and V beam pattern differences, presented in the right panel of Fig. 9, illustrates the improvement and is discussed next.

A qualitative comparison of copolar pattern differences in the panels of Fig. 9 indicates that H and V beams are considerably better matched. That is, comparing the values inside the -3 dB beamwidths (dotted black lines), it can be seen that differences are close to 0 dB after the back-projection calibration. Nevertheless, some assumptions are made when emulating the back-projection calibration method here. First, it is likely that the response of the array electronics (specially amplifiers) will not be perfectly linear when applying the back-projection correction values at the element level. Achieving a high level of beam matching would likely entail an iterative back-projection calibration following a "hardware-in-the-loop" type approach. Second, the patterns derived here are based on applying back-projection corrections at the element level and re-projecting the fields forward, which omit diffraction changes. That is, the analysis presented here quantifies the performance of back-projection calibration using a hybrid measurement/simulation approach, whereby initial measurements are actual but those after applying the calibration are simulated. Considering that the back-projection correction values are small, we would expect relatively minor changes in diffraction fields when re-measuring patterns. These would also be accounted for in the iterative process discussed. Lastly, considering magnitude and phase noise in the array, it is

likely that back-projection calibration would not result in numerically precise calibration but rather overall statistically accurate (assuming uncorrelated noise). Since the Horus array has 16-bit digital-to-analog converters, at the front end before the antenna, we expect noise levels to be small. Having these considerations in mind, we believe that the back-projection method could help achieve high-fidelity calibration of Horus.

We introduce the *beam mismatch contamination* (BMC) as a metric to quantify the performance of the back-projection calibration method. The BMC is defined as the integral of the absolute copolar pattern differences over the half-power beamwdith,

$$BMC(\theta, \phi) = \int_{\theta \in \Theta_3} \int_{\phi \in \Phi_3} \left| 10 \log_{10}\left[\frac{F_{hh}^2}{F_{vv}^2} \right] \right| \sin(\theta) d\theta d\phi, \quad (8)$$

where $\Theta_3 = \{ \theta \in \mathbb{R} \mid F_{hh}^2(\theta, \phi) > 0.5 \}$, $\Phi_3 = \{ \phi \in \mathbb{R} \mid F_{hh}^2(\theta, \phi) > 0.5 \}$, and F_{hh} and F_{vv} are the copolar H and V magnitude patterns. Note that BMC evaluates differences over the region determined by the copolar H pattern half-power beamwidth (i.e., Θ_3 and Φ_3), therefore the area normalization factor cancels out as it is in both terms in the ratio F_{hh} and F_{vv}. For the broadside beams, the BMC values before and after back-projection calibration are 0.13 dB and 0.04 dB. Next, we investigate the performance of the back-projection calibration as a function of electronic beamsteering.

B. Electronically Scanned Beams

It is known that co- and cross-polar antenna patterns of polarimetric PAR induce biases in the polarimetric variables,
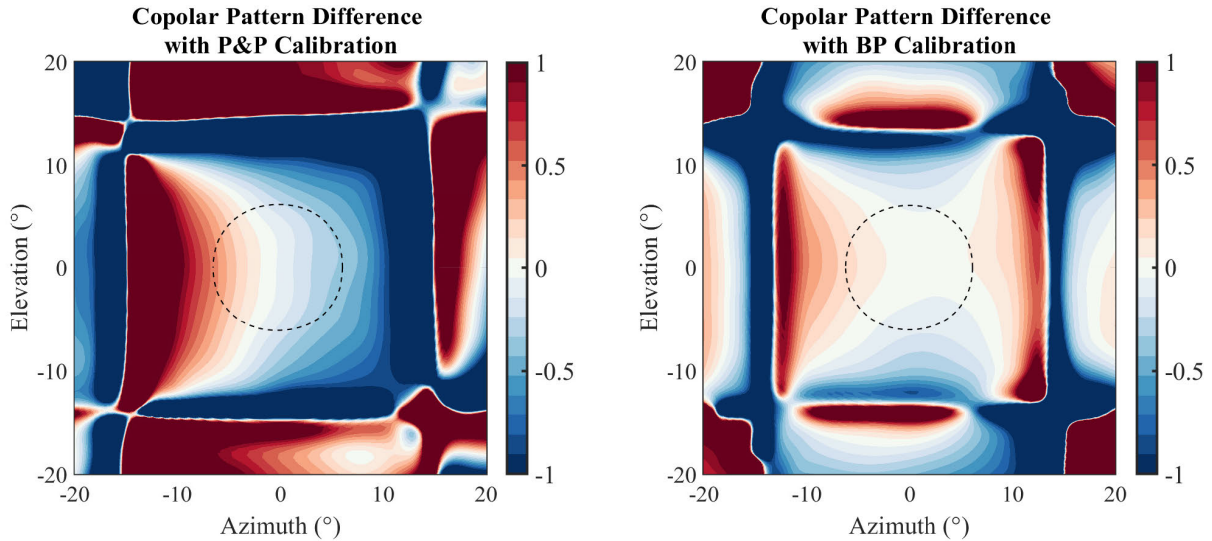
Fig. 9. Difference in measured Horus H and V beam patterns (H - V in dB) for (left) park & probe calibration, (right) back-projection calibration. This metric quantifies how well the H and V beams are matched at broadside. Dotted black contours represents the -3 dB width of the copolar H pattern.
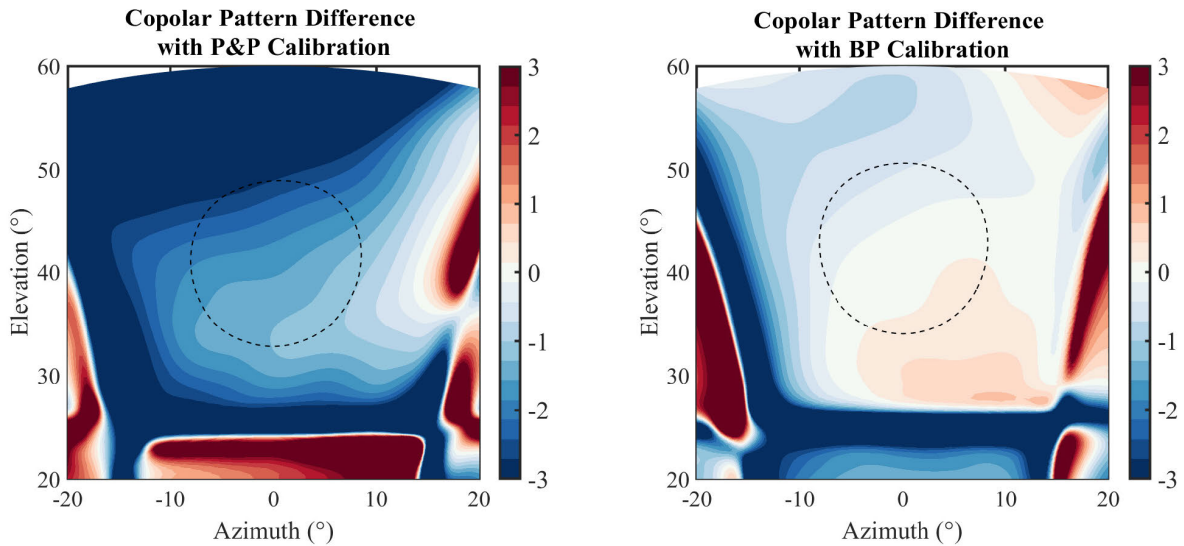

Fig. 10. Same plots as shown in Fig. 9 but for beams scanned to $42°$ in elevation.

which increase as the beam is steered away from the broadside. The Horus 8×8 array was configured to scan beams in elevation, from $-42°$ to $42°$ in steps of $6°$. Near-field patterns were measured for every steering angle and processed using the back-projection calibration method. The resulting pattern differences for the beams scanned at $42°$ elevation are shown in Fig. 10.

Considering the left panel in Fig. 10, it can be seen that, as expected, the element pattern roll-off factor is lower in V than in H along the elevation dimension. That is, as the beam is steered upwards in elevation, power from the vertical polarization beam is higher than the horizontal, hence the negative difference values. A qualitative comparison shows that copolar differences are much lower when using the back-projection calibration. In this case, element magnitudes in the vertical polarization are generally lowered by the back-projection calibration algorithm to equalize powers across the

array and match the formed H and V beams. While this helps mitigate the scan loss incurred when steering the beam off broadside and improve polarimetric calibration, it results in a small gain loss. These gain losses vary as a function of steering angle as shown in Fig. 11. Nevertheless, this demonstrates that the back-projection algorithm can be used to approximately match off-broadside H/V beams. In this case, the BMC values before and after back-projection calibration are 0.34 dB and 0.05 dB.

The maximum BMCs obtained with the park & probe and back-projection calibration methods are 0.34 and 0.08 dB across all 15 scanned beams. These results seem very encouraging and indicate the potential of this method to achieve strict H/V beam matching performance needed for accurate weather observations. Nevertheless, it is important to evaluate the robustness of the back-projection method to excitation magnitude and phase errors.
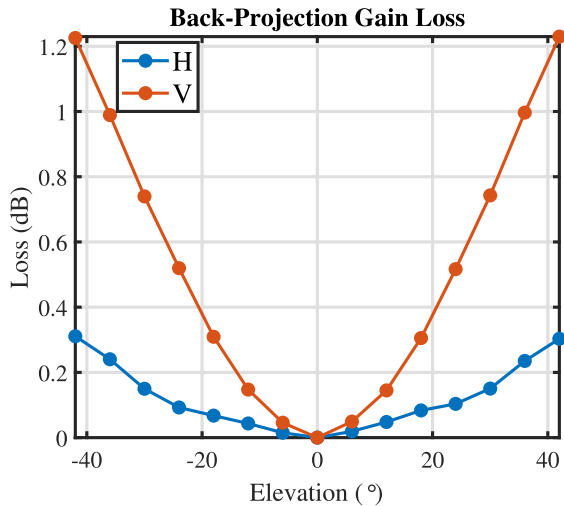
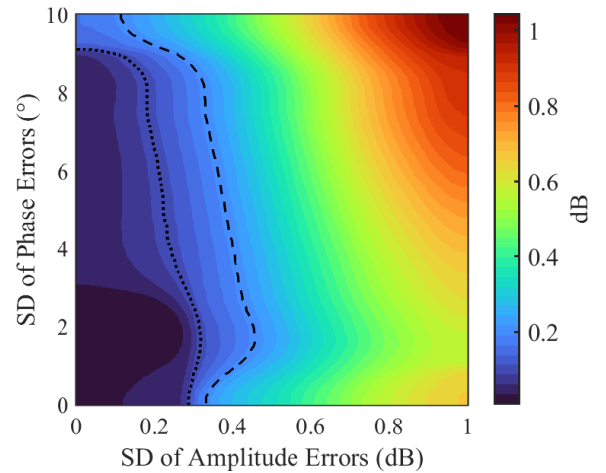Fig. 11. Gain loss incurred when using BP calibration to match H/V beams.

Fig. 12. Robustness of back-projection calibration to excitation amplitude and phase errors. Contour plots indicate the 0.1 dB (dotted) and 0.2 dB (dashed) beam matching levels.

VI. ROBUSTNESS ANALYSIS

Herein, we analyse the robustness of the polarimetric back-projection calibration as a function of excitation amplitude and phase errors. These errors are systematically simulated for each element and each polarization independently using zero-mean Gaussian distributions. For the magnitude, fluctuations with standard deviation (STD) from 0 to 1 dB in steps of 0.01 dB are added to the excitations after applying the initially derived back-projection calibration corrections from actual near-field measurements. A similar procedure is carried out for the phase errors, from 0° to 10° in steps of 0.1°.

The H/V beam matching of the resulting simulated far-field patterns is quantified using (8), and presented in Fig. 12. Results show that for relatively high errors in the amplitude and phase of excitations, the mean copolar pattern differences could be larger than 1 dB. This would certainly be unacceptable for quantitative precipitation estimation products derived from polarimetric radar measurements [35]. We expect this calibration method to be more effective with fully-digital arrays, given the high precision of front-end digital electronic components. For the Horus radar, the AD9371 digital receiver is rated to sample up to 125 MSPS, and produces baseband in-phase (I) and quadrature (Q) digital signals with 16-bit sampling, which are mapped into a word of two bytes [21]. Although we do not have sufficient data for a quantitative analysis of excitation stability, recent measurements have very small excitation drifts (i.e., < 0.25 dB and $< 0.8°$ in amplitude and phase) with respect to measurements taken six months earlier. We plan to investigate excitation stability in the near future, once the full Horus array is completed.

It is apparent from these results that the back-projection calibration is robust to phase noise, as it can maintain an overall good beam matching level proven by the BMC. In contrast, it seems to be sensitive to the amplitude fluctuations, as moderate errors (STD$\sim$0.4 dB) can result in considerable biases (BMC$\sim$0.3 dB). Note that this metric may be more sensitive to amplitude fluctuations because it only accounts for absolute differences in copolar patterns within the half power beamwidth. An investigation on biases induced in the phase (e.g., Φ_{DP}) is beyond the scope of this article.

Contour plots in Fig. 12 indicate the 0.1 dB (dotted) and 0.2 dB (dashed) beam matching levels, the first one being ideal and the second acceptable [22]. Based on this results, we can see that it would only be effective on systems with relatively high precision for excitation control, and assuming high-resolution near-field measurements. This is one of the limitations for using the holographic back-projection to perform radar calibration [36]. Nevertheless, new fully-digital PARs such as the Horus system are equipped with 16-bit precision DACs in the front end, and can produce accurate excitations. We used the near-field measurements discussed previously to estimate the standard deviation of amplitude and phase errors for the Horus panel and found them to be 0.221 dB and 1.954°. These promising results indicate that holographic back-projection calibration could be a viable option for achieving strict polarimetric calibration needs for meteorological observations.

VII. CONCLUSION

This article presents a new calibration method for the all-digital Horus polarimetric phased array radar. Horus is a polarimetric, S-band phased array radar developed at the ARRC with support from NOAA [21]. Its antenna aperture is composed of a 5×5 arrangement of panels (of which not all are active), each with 8×8 antenna elements. With 1024 active elements in total, this proof-of-concept all digital system will have a 3-dB beamwidth of $\sim 4°$. Although back-projection-based phase calibration has been considered before, it has not been used for fully-digital polarimetric radar calibration of excitation amplitudes and phases to improve H/V beam matching. In addition, this article evaluates the effectiveness of polarimetric back-projection calibration for broadside and electronically steered beams. A robustness analysis was conducted to evaluate the back-projection calibration as a function of random excitation errors, through a new quantitative metric (i.e., BMC).

The proposed back-projection calibration requires a planar near-field scanner with enough dynamic range to record a difference between the maximum and minimum signal

larger than 40 dB, and with the capability to measure cross-polarization fields. The measurements in the near-field are projected back onto the array plane to get the electric-field intensities and phases of each element. These are digitally adjusted to eliminate variations across the aperture. Then the fields are projected to the far-field to remove the effects from the probe. The linear ratio of H and V (i.e., their difference in dB) is used as a metric to evaluate copolar H/V beam matching. As shown in Section V, this results in significantly improved H/V beam matching. The beam mismatch contamination metric is defined to quantify the matching of the Horus panel copolar beam patterns at different electronically scanned angles. For broadside, the BMC values before (i.e., park and probe) and after back-projection calibration measured are 0.13 dB and 0.04 dB. The maximum BMCs obtained with the park & probe and back-projection calibration methods are 0.34 and 0.08 dB across all scanned beams. These encouraging results show the potential of this method to achieve strict H/V beam matching performance needs for accurate weather observations. There is, however, a small gain loss incurred and it is approximately proportional to the array scan loss.

It is important to note the performance relies on linearity of the amplifiers operating near saturation, array stability, and the precision of the element-level excitations. Although the back-projection calibration is only evaluated for a single panel, we plan to test it with the full Horus array of 5×5 panels in the near future. Because a larger aperture will result in a narrower beamwidth, we argue that H/V beam mismatches are mainly driven by the embedded element patterns and thus will not change the BMC significantly.

The installation and testing of a sufficiently large near-field scanner was recently completed in the ARRC facilities. Several key properties of the scanner include: planarity of < 0.1 mm, corrected planarity of < 0.05 mm RMS, and x-y resolution < 0.0375 mm. Hence, this scanner will enable Horus's key performance parameters to be accurately measured, including: full two-dimensional co- and crosspolar near-field patterns from which gain, sidelobe levels, beam pointing accuracy, beamwidth, crosspolar isolation, and null depths, can be extracted. The scanning plane is 20 ft. by 20 ft. The scanner supports frequencies from the upper end of the L-band through Ka-band, and it is currently the largest university-based near-field scanner in the nation. Fig. 13 depicts a line drawing of Horus within the new near-field scanner. Additional work is underway to interface the scanner with the full Horus array and ensure signal synchronization. Once the scanner is ready later this year, we will implement the back-projection calibration on the full array.

Potential advantages of this method include the possibility to calibrate a polarimetric array without the need for an external far-field probe, fast calibration over large bandwidths, and higher accuracy in H/V beam matching. Polarimetric calibration can be conducted measuring far-field patterns to digitally compensate for mismatches and amplitude and phase imbalances. However, deploying a far-field measurement probe and getting uncontaminated samples in the presence of multi-path and external interference can be challenging. Large bandwidths could be measured by sweeping a desired frequency
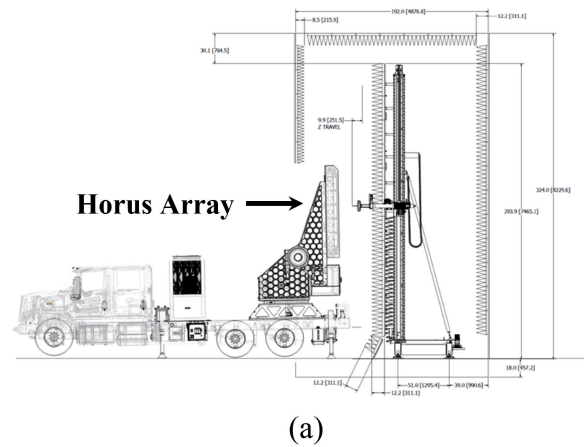
(a)

(b)

Fig. 13. Near-field scanner recently installed at the ARRC for measuring full Horus array patterns (a) schematic (b) photograph. The scanning plane is 20 ft by 20 ft, and it supports frequencies from the upper end of the L-band through Ka-band.

range while collecting near-field samples and independently post-processing each frequency to produce back-projection calibration lookup tables. Lastly, if most of the electric-field energy is appropriately sampled in an uncontaminated near-field environment, and the array is sufficiently stable, the corrections derived could provide high levels of H/V beam matching. This naturally improves measurements accuracy by mitigating antenna-induced biases in meteorological estimates. Although in this article we focus on the radar meteorology application, we point out that back-projection calibration would be equally beneficial to other PAR applications, including those that only require single polarization measurements. Back-projection calibration would be especially beneficial for applications requiring high bandwidth signals, such as air surveillance and defense.

ACKNOWLEDGMENT

REFERENCES

[1] D. Zrnić, R. Doviak, G. Zhang, and A. Ryzhkov, "Bias in differential reflectivity due to cross coupling through the radiation patterns of polarimetric weather radars," *J. Atmos. Ocean. Technol.*, vol. 27, no. 10, pp. 1624–1637, Oct. 2010, doi: 10.1175/2010JTECHA1350.1.

[2] NOAA/NWS. (2015). *Radar Functional Requirements*. [Online]. Available: https://roc.noaa.gov/WSR88D/PublicDocs/NOAA_Radar_Functional_Requirements_Final_Sept%202015.pdf

[3] Y. Pointin, D. Ramond, and J. Fournet-Fayard, "Radar differential reflectivity ZDR: A real-case evaluation of errors induced by antenna characteristics," *J. Atmos. Ocean. Technol.*, vol. 5, no. 3, pp. 416–423, Jun. 1988.

[4] N. Balakrishnan and D. S. Zrnic, "Use of polarization to characterize precipitation and discriminate large hail," *J. Atmos. Sci.*, vol. 47, no. 13, pp. 1525–1540, Jul. 1990.

[5] M. Weber et al., "Towards the next generation operational meteorological radar," *Bull. Amer. Meteorolog. Soc.*, vol. 102, no. 7, pp. E1357–E1383, Jul. 2021.

[6] M. Sarcione et al., "The design, development and testing of the THAAD (theater high altitude area defense) solid state phased array (formerly ground based radar)," in *Proc. Int. Symp. Phased Array Syst. Technol.*, 1996, pp. 260–265.

[7] I. Ivic et al., "An overview of weather calibration for the advanced technology demonstrator," in *Proc. IEEE Int. Symp. Phased Array Syst. Technol. (PAST)*, Oct. 2019, pp. 1–7.

[8] I. Ivić and D. Schvartzman, "A first look at the ATD data corrections," in *Proc. 39th Int. Conf. Radar Meteorol.*, 2019, pp. 2–6.

[9] H. M. Aumann and F. G. Willwerth, "Phased-array calibration by adaptive nulling," MIT Lincoln Lab., Cambridge, MA, USA, Tech. Rep. 915, 1991. [Online]. Available: https://www.ll.mit.edu/r-d/publications/phased-array-calibration-adaptive-nulling

[10] D. J. Wasielewski, I. R. Ivic, J. R. Mendoza, and F. A. Zahrai, "Implementation of a far-field tower for calibrating a dual-polarization planar phased-array radar," in *Proc. 100th Amer. Meteorolog. Soc. Annu. Meeting*, 2020.

[11] A. Y. Umeyama, J. L. Salazar-Cerreno, and C. Fulton, "UAV-based antenna measurements for polarimetric weather radars: Probe analysis," *IEEE Access*, vol. 8, pp. 191862–191874, 2020.

[12] A. R. Segales et al., "Development of a technique for scanning antenna patterns using unmanned aircraft systems," in *Proc. 103rd AMS Annu. Meeting*, 2023.

[13] C. Fulton et al., "Mutual coupling-based calibration for the Horus digital phased array radar," in *Proc. IEEE Int. Symp. Phased Array Syst. Technol. (PAST)*, Oct. 2022, pp. 1–6.

[14] I. R. Ivić and D. Schvartzman, "Weather calibration efforts on the advanced technology demonstrator," in *Proc. 100th Amer. Meteorolog. Soc. Annu. Meeting*, 2020

[15] W. D. Zittel, J. G. Cunningham, R. R. Lee, L. M. Richardson, R. L. Ice, and V. Melnikov, "Use of hydrometeors, Bragg scatter, and sun spikes to determine system ZDR biases in the WSR-88D fleet," in *Proc. 8th Eur. Conf. Radar Meteorol. Hydrol.*, vol. 12, 2014.

[16] L. M. Richardson, W. D. Zittel, R. R. Lee, V. M. Melnikov, R. L. Ice, and J. G. Cunningham, "Bragg scatter detection by the WSR-88 D. Part II: Assessment of ZDR bias estimation," *J. Atmos. Ocean. Technol.*, vol. 34, no. 3, pp. 479–493, Mar. 2017.

[17] A. C. Newell, B. Schluper, and R. J. Davis, "Holographic projection to an arbitrary plane from spherical near-field measurements," in *Symp. Dig. Antenna Meas. Techn. Assoc.*, 2001, pp. 92–97.

[18] K. Hassett, "Phased array antenna calibration measurement techniques and methods," in *Proc. Eur. Conf. Antennas Propag. (EuCAP)*, 2016, pp. 1–4.

[19] J. T. Logan, D. S. Reinhard, and K. E. Hauck, "Phased array calibration and diagnostics utilizing a student-built planar near-field system," in *Proc. IEEE Int. Symp. Phased Array Syst. Technol.*, Oct. 2010, pp. 279–286.

[20] D. Schvartzman et al., "A polarimetric antenna-calibration method for the Horus radar based on E-field back projection," in *Proc. IEEE Int. Symp. Phased Array Syst. Technol. (PAST)*, Oct. 2022, pp. 01–07.

[21] R. D. Palmer et al., "Horus—A fully digital polarimetric phased array radar for next-generation weather observations," *IEEE Trans. Radar Syst.*, vol. 1, pp. 96–117, 2023. [Online]. Available: https://ieeexplore.ieee.org/document/10136237, doi: 10.1109/TRS.2023.3280033.

[22] D. Zrnić, D. Schvartzman, R. D. Palmer, and A. Ryzhkov, "Effects of Horus antenna patterns on the copolar correlation of weather returns," *IEEE Trans. Radar Syst.*, early access, Jun. 7, 2023, doi: 10.1109/TRS.2023.3283560.

[23] R. Palmer et al., "A primer on phased array radar technology for the atmospheric sciences," *Bull. Amer. Meteorolog. Soc.*, vol. 2022, pp. 1–15, Jan. 2022. [Online]. Available: https://journals.ametsoc.org/view/journals/bams/aop/BAMS-D-21-0172.1/BAMS-D-21-0172.1.xml

[24] R. D. Palmer et al., "Horus—An all-digital phased array weather radar developed at the University of Oklahoma," in *Proc. 103rd AMS Annu. Meeting*, 2023.

[25] J. D. Díaz, "Ultra-low cross-polarization antenna architectures for multi-function planar phased arrays," Ph.D. dissertation, Dept. Elect. Comput. Eng., Univ. Oklahoma, Norman, OK, USA, 2021. [Online]. Available: https://hdl.handle.net/11244/330113

[26] C. Fulton, M. Yeary, D. Thompson, J. Lake, and A. Mitchell, "Digital phased arrays: Challenges and opportunities," *Proc. IEEE*, vol. 104, no. 3, pp. 487–503, Mar. 2016.

[27] C. A. Balanis, *Antenna Theory: Analysis and Design*. Hoboken, NJ, USA: Wiley, 2015.

[28] G. F. Masters, "Probe-correction coefficients derived from near-field measurements," in *Proc. Antenna Meas. Techn. Assoc. Symp.*, 1991, pp. 1–10.

[29] C. A. Balanis, *Antenna Theory: Analysis and Design*, 2nd ed. Hoboken, NJ, USA: Wiley, 2005.

[30] J. A. Ortiz, "Impact of edge diffraction in dual-polarized phased array antennas," Ph.D. dissertation, Dept. Elect. Comput. Eng., Univ. Oklahoma, Norman, OK, USA, 2020. [Online]. Available: https://shareok.org/handle/11244/325369

[31] D. Garneski, "A new implementation of the planar near-field back projection technique for phased array testing and aperture imaging," in *Symp. Dig. The Antenna Meas. Techn. Assoc.*, 1990, p. 9.

[32] L. J. Foged, F. Mioc, and A. Rosa, "Applicability investigation of holographic back-projection of spherical near field measured data," in *Proc. 1st Eur. Conf. Antennas Propag.*, Nov. 2006, pp. 1–6.

[33] S. Gregson, J. McCormick, and C. Parini, *Principles of Planar Nearfield Antenna Measurement*, vol. 53. Edison, NJ, USA: IET, 2007.

[34] A. C. Newell, "Estimating the uncertainties due to truncation in planar near-field holograms," in *Proc. AMTA Conf.*, 2004, pp. 1–6.

[35] A. Ryzhkov and D. Zrnic, *Radar Polarimetry for Weather Observations* (Springer Atmospheric Sciences). Cham, Switzerland: Springer, 2019. [Online]. Available: https://books.google.com/books?id=d0uYvQEACAAJ

[36] D. J. van Rensburg, "Limitations of near-field back projection for phased array tuning applications," in *Proc. AMTA*, 2001, pp. 1–5.
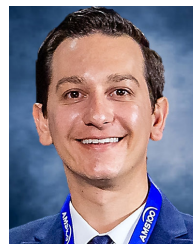
David Schvartzman (Senior Member, IEEE) was born in Piracicaba, Brazil, in 1988. He received the B.S. degree in electrical and computer engineering from the National University of Asunción, San Lorenzo, Paraguay, in 2011, and the M.S. and Ph.D. degrees in electrical and computer engineering from The University of Oklahoma, Norman, OK, USA, in 2015 and 2020, respectively.

From 2015 to 2020, he was a Research Scientist with the NOAA National Severe Storms Laboratory (NSSL) and the Cooperative Institute for Severe and High-Impact Weather Research and Operations (CIWRO). From 2021 to 2022, he was a Research Scientist with the Advanced Radar Research Center (ARRC), The University of Oklahoma, where he is currently an Assistant Professor with the School of Meteorology, affiliated with the ARRC. He is also an Adjunct Assistant Professor with the School of Electrical and Computer Engineering, The University of Oklahoma. He works on novel signal and array processing algorithms to improve understanding of atmospheric processes using phased array radar. He also works on calibration and integration of phased array radar systems. He is a member of the American Meteorological Society (AMS). He was a recipient of the 2019 American Meteorological Society's Spiros G. Geotis Prize and the 2022 IEEE R5 Outstanding Young Professional Award.

Jose D. Diaz Diaz received the B.Sc. degree in electrical engineering with a minor in atmospheric sciences and meteorology from the University of Puerto Rico at Mayagüez, Mayagüez, Puerto Rico, in 2015, and the M.S. and Ph.D. degrees in electrical engineering from The University of Oklahoma (OU), Norman, OK, USA, in 2018 and 2021, respectively. From 2018 to 2021 he was a full-time Radar Engineer working on all-digital phased array radar systems with the Advanced Radar Research Center (ARRC). Since 2021, he has been a Senior Radar Systems Engineer with the Johns Hopkins University (JHU) Applied Physics Laboratory (APL) Air and Missile Defense Sector (AMDS). His research interests include the design of high-performance antenna elements for phased-array radars and their calibration.
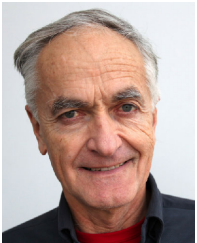
Dušan Zrnić (Life Fellow, IEEE) received the bachelor's degree from the University of Belgrade, Belgrade, Serbia, in 1965, and the M.S. and Ph.D. degrees from the University of Illinois at Urbana–Champaign, Champaign, IL, USA, in 1966 and 1969, respectively.

He is currently a Senior Scientist with the National Severe Storms Laboratory, Norman, OK, USA, and an Affiliate Professor of meteorology and electrical engineering with The University of Oklahoma, Norman. He has developed several scientific and engineering aspects of polarimetric weather radar technology leading to implementation on the WSR-88Ds. He was inducted into the U.S. National Academy of Engineering in 2006 for the development of potent radar methods that have greatly enhanced operational weather detection and warning and advanced meteorological research. He is currently a fellow of AMS. He was a recipient of the AMS Remote Sensing Prize in 2008 for pioneering and substantial contributions to the improvements of meteorological radars for both research and operational applications. He was the Chief Editor of the *Journal of Atmospheric and Oceanic Technology*.

Matthew Herndon (Member, IEEE) received the B.S. degree (Hons.) (magna cum laude) in computer engineering and the M.S. degree in electrical and computer engineering from The University of Oklahoma, Norman, OK, USA, in 2017 and 2022, respectively, where he is currently pursuing the degree. In 2017, he joined the Advanced Radar Research Center (ARRC), The University of Oklahoma. He has contributed to variety of projects as a full-time Radar Engineer. He specializes in phased array systems, signal processing, and FPGA/software architecture and system design. He received the *ARRC Journal* Paper Award in 2021.

Mark B. Yeary (Fellow, IEEE) received the Ph.D. from the Department of Electrical Engineering, Texas A&M University, College Station, TX, USA, in 1999.

Since Fall 2002, he has been with the School of Electrical and Computer Engineering, The University of Oklahoma (OU), Norman, OK, USA, where he was named the endowed Hudson-Torchmark Presidential Professor in 2011. As of 2005, he is also a Founding Member of the Advanced Radar Research Center (ARRC), OU, which is the largest university-based radar center in the nation. For instance, he was deeply involved in the National Weather Radar Testbed, the ARRC's Atmospheric Imaging Radar program, and the ARRC's Horus program. He has served as a PI or Co-PI on grants from ONR, NASA, NSF, NOAA, and DARPA. His research interests include digital signal processing and radar systems with an emphasis on hardware prototype development.

Prof. Yeary is a fellow of the Cooperative Institute for Severe and High-Impact Weather Research and Operations (CIWRO), National Weather Center, Norman. In 2022, he was awarded OU's George Lynn Cross Research Professorship and named the Gallogy Chair Professorship within OU's Gallogly College of Engineering. He serves as a Faculty Advisor to OU's American Indians in Science and Engineering Society (AISES) Chapter. He served as the Co-Chair for the 2018 IEEE Radar Conference. Since 2009, he has been the Chair of the Radar Sessions at the American Meteorological Society (AMS) Annual Meetings. He is a licensed Professional Engineer.

Robert D. Palmer (Fellow, IEEE) was born in Fort Benning, GA, USA, in 1962. He received the Ph.D. degree in electrical engineering from The University of Oklahoma (OU), Norman, OK, USA, in 1989.

From 1989 to 1991, he was a JSPS Post-Doctoral Fellow with the Radio Atmospheric Science Center, Kyoto University, Japan, where his major accomplishment was the development of novel interferometric radar techniques for studies of atmospheric turbulent layers. After his stay in Japan, he was with the Department of Physics and Astronomy, Clemson University, South Carolina. From 1993 to 2004, he was a part of the faculty of the Department of Electrical Engineering, University of Nebraska–Lincoln, where his interests broadened into areas, including wireless communications, remote sensing, and pedagogy. Soon after moving to OU as the Tommy C. Craighead Chair with the School of Meteorology in 2004, he established the interdisciplinary Advanced Radar Research Center (ARRC). He currently serves as the Executive Director of the ARRC and OU's Associate Vice President for Research andPartnerships. While at OU, his research interests have focused on the application of advanced radar signal processing techniques to observations of severe weather, particularly related to phased-array radars and other innovative system designs. He has published widely in the area of radar sensing of the atmosphere, with more than 115 peer-reviewed journal articles, one textbook, 40 international invited talks, and more than 300 conference presentations.

Prof. Palmer is a fellow of the American Meteorological Society (AMS) emphasizing his dedication to the interdisciplinary nature of radar science.